Superhydrophobic and high SERS performance of Ag coated CuO nanostructured thin films prepared by successive ionic layered...

Article *in* Journal of Colloid and Interface Science · May 2016

DOI: 10.1016/j.jcis.2016.05.051

CITATION
1

READS
141

6 authors, including:

Dhanpal Naidu
Indian Institute of Science
8 PUBLICATIONS **24** CITATIONS
SEE PROFILE

Sonia S
Holy Cross College (Autonomous), Nagercoil
9 PUBLICATIONS **54** CITATIONS
SEE PROFILE

Palaniswamy Suresh Kumar
Center of Innovation, Singapore
64 PUBLICATIONS **1,713** CITATIONS
SEE PROFILE

Mohan rao Gowravaram
Indian Institute of Science
185 PUBLICATIONS **2,058** CITATIONS
SEE PROFILE

Journal of Colloid and Interface Science 477 (2016) 209–219

Contents lists available at ScienceDirect

Journal of Colloid and Interface Science

journal homepage: www.elsevier.com/locate/jcis

Regular Article

Analysis on superhydrophobic silver decorated copper Oxide nanostructured thin films for SERS studies

Naidu Dhanpal Jayram [a,b], D. Aishwarya [a], S. Sonia [a,c], D. Mangalaraj [a,*], P. Suresh Kumar [d], G. Mohan Rao [e]

[a] Department of Nanoscience and Technology, Bharathiar University, Coimbatore 641 046, India
[b] Department of Science and Humanities, KIT-Kalaignar Karunanidhi Institute of Technology, Kannampalayam, Coimbatore, Tamil Nadu 641402, India
[c] Department of Physics, Holy Cross College (Autonomous), Nagercoil 629004, India
[d] Environmental & Water Technology, Centre of Innovation, Ngee Ann Polytechnic, Singapore 599489, Singapore
[e] Plama Processing Lab, Department of Instrumentation and Applied Physics, Indian Institute of Science, Bangalore 560012, India

GRAPHICAL ABSTRACT

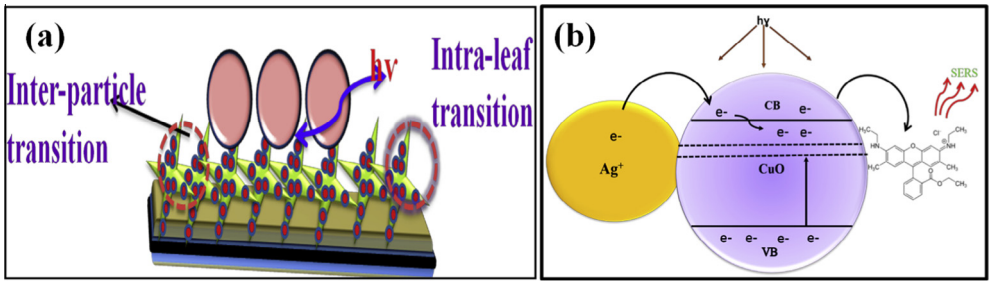

ARTICLE INFO

Article history:
Received 3 April 2016
Revised 22 May 2016
Accepted 24 May 2016
Available online 25 May 2016

Keywords:
Ag@CuO
Nanoflowers
SILAR
Superhydrophobic
Rhodamine 6G

ABSTRACT

The present work demonstrates the superhydrophobic and Surface Enhanced Raman Spectroscopy (SERS) active substrate performance of silver coated copper oxide (Ag@CuO) nanostructured thin films prepared by the SILAR process. Super hydrophobic substrates that combine super hydrophobic condensation effect and high enhancement ability of Ag@CuO nanoflowers are investigated for SERS studies. The possible growth mechanism for the formation of nanoflower arrays from nanospindles has been discussed. Morphology and crystallinity of the Ag@CuO thin films are confirmed using FESEM and XRD. The results obtained in the present study indicate that the as-deposited hydrophobic nanospindles structure converts to super hydrophobic nanoflower arrays on annealing at 200 °C. The Ag@CuO super hydrophobic nanoflowers thin film based SERS substrates show highly enhanced Raman spectra with an EF value of 2.0×10^7 for (Rhodamine 6G) R6G, allowing a detection limit from a 10^{-10} mol L^{-1} solution. The present study may provide a new perception in fabricating efficient super hydrophobic substrates for SERS, suggesting that the fabricated substrates are promising candidates for trace analysis of R6G dye and are expected to be widely used as highly sensitive SERS active substrates for various toxic dyes in the future.

1. Introduction

Superhydrophobic surfaces are fascinating in view of their widespread and potential applications in various industrial fields and in self-cleaning processes such as in drug delivery, anticorrosion, and lab-on-chip systems. Their performance can be controlled by well-mannered nanostructures and chemical composition of solid surfaces [1]. In addition to the above applications they have also been used for Surface Enhanced Raman studies (SERS) [2,3]. One of the most dynamic research fields in SERS is related to the search for new substrates with improved enhancement efficiency,

* Corresponding author.
E-mail addresses: dhanpal.dj@gmail.com, dmraj800@yahoo.com (D. Mangalaraj).

http://dx.doi.org/10.1016/j.jcis.2016.05.051
0021-9797/

reproducibility and stability [4]. During the past few decades, there has been a significant development of SERS active substrates. Noble metals and transition metals, such as Ag, Au, Cu, Pd, Co, and Ni, have been widely employed to obtain a higher value of the enhancement [5]. Metal oxides have also been investigated as SERS substrates as they are used in many applications. However, it is found that the direct SERS activity of metal oxide semiconductors is much lower than that of noble metals. Hence it is essential to further improve the SERS activity of these semiconductors for practical applications. Semiconductor/noble metal nanocomposites exhibit a strong Raman enhancement associated with tuning of the Localized Surface Plasmon Resonance (LSPR) of the metallic nanoparticles, inducing a charge transfer (CT) effect at the semiconductor/metal interface [6]. Various metal oxides, namely TiO_2, CuO and SiO_2 were modified by coating with Ag, resulting in improved SERS effect [7–9]. Thus there is a great opportunity in the near future for the development and engineering of metal oxide nanostructure-based SERS substrates [10,11].

Metal oxides like ZnO, TiO_2, SnO_2 and WO_3, which are n-type semiconductors, have been generally widely used in the form of nanostructured thin films. However, p-type semiconductors exhibit wider applications when compared to the n-type semiconductors. Copper oxide (CuO), an important p-type semiconductor with a narrow band gap of 1.21 eV, has attracted great interest recently due to its wide applications in sensors, magnetic storage media, solar-energy transformers, electronics devices and in catalysis [12–14]. CuO nanocrystals especially, are frequently employed as photochemically active and photoconductive compounds. Compared to Cu_2O, CuO thin films show higher stability and reproducibility which is a major criterion for device fabrication. A report by Wang and his co-workers shows Enhanced Raman scattering from 4-Mpy molecules adsorbed on CuO nanocrystals [15]. Till date, there are only a few reports available on Ag@CuO nanocomposites for surface enhanced Raman scattering (SERS). Mao et al. [16] demonstrated that the metal-semiconductor (Ag-CuO) contact can alter the charge distribution through p-aminothiophenol (PATP) molecules. When CuO was junctioned with Ag nanoparticles, charge transfer occurred from the CuO to the Ag nanoparticles, inducing a larger electromagnetic field [17]. Hence, Ag nanoparticles could excite a more stable and intense localized surface plasmonic resonance under laser irradiation. A similar result has been reported by Hsieh et al. [17] for the improvement of the SERS activity of solution-phase Ag@CuO nanocomposites as a function of Ag content, using 4 aminothiophenol (4-ATP) as the probe molecule. The enhancement on Ag@CuO nanocomposites may be attributed to the charge transfer transition between the semiconductor and metallic nanoparticles. Even though these reports have shown good response towards the Ag@CuO and Cu nanoparticle-coated CuO nanocomposites [18], there are a few problems which have not been discussed till date. One of the basic and natural problems with Copper films is its oxidizing state, which affects the stability of the CuO films. Similarly the interdependence of SERS and nanostructures has not been discussed for copper oxide films. The present work shows the role of superhydrophobic surfaces in SERS studies and deals with the preparation of stable copper oxide thin films for obtaining stronger SERS using Ag@CuO nanoflowers array through a low cost method. It also discusses the role of interdependence of Raman spectra and SEM morphology.

2. Experimental section

2.1. Synthesis of cupric oxide thin films using SILAR method

Superhydrophobic surfaces of Copper Oxide (CuO) nanostructures have been designed by SILAR process as reported for Zinc Oxide (ZnO) [19] and CuO in our previous work [20]. The procedure for this method is schematically represented in Fig. 1. The detailed experimental procedure and reaction mechanism have been discussed in the previous work [20]. The successive cycles and the increase in the deposition times led to an increase in thickness of the deposited film. The reaction cycle was repeated 20, 40 and 60 times. Silver was deposited for SERS studies using thermal evaporation from a helical coil onto the CuO nanostructure for a deposition time of 2 min. The film was annealed at 200 °C and silver were again deposited; the desired parameter was chosen from the previous publication and resulted in the formation of silver decorated nanoflower like structure [3,20]. The thickness of the deposited silver film was recorded using a quartz crystal thickness monitor.

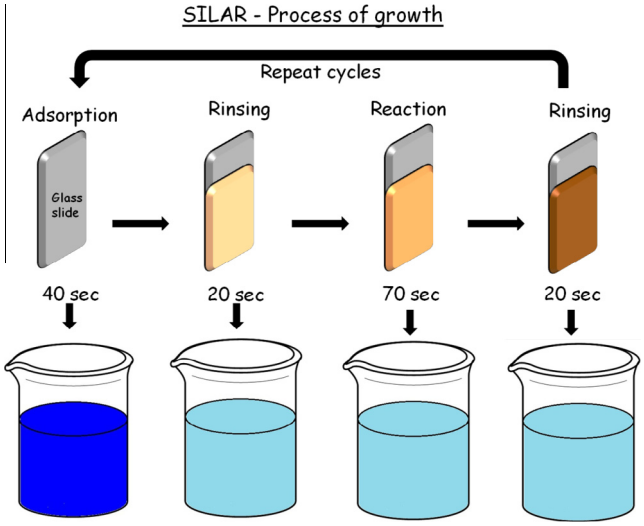

Fig. 1. Schematic illustration of growth of CuO thin films by SILAR method.

2.2. Characterization techniques

Ag@CuO nanostructured thin films were characterized using the following techniques. X-ray diffraction (XRD) patterns were obtained using a Panalytical X'Pert Pro with Cu K_α radiation (1.5406 Å), absorbance spectra were analyzed using UV–Vis spectrometer (JascoV-640) and morphological details through FE-SEM (quanta-250). SERS spectra were recorded using Raman spectrometer (LABRAM-HR) with laser excitation lines of 514 nm at room temperature. X-ray photoelectron spectra were recorded using (Kratos analytical, ESCA-3400, Shimadzu). The super hydrophobicity and the contact angle measurements of the substrate were carried out at room temperature using a contact angle meter. Contact angle measurements were recorded using the sessile drop method (about 2 µl distilled water droplet) with a video-based drop shape analyzer (FTA 135, First Ten Angstroms, Portsmouth, VA) placed on different locations of the coated and uncoated samples.

3. Results and discussion

3.1. Structural analysis

X-ray diffraction (XRD) patterns were recorded for the copper oxide thin films prepared with 20, 40 and 60 cycles of deposition. The diffraction pattern in Fig. 2(a) for the as-prepared film depicts the preferred orientation plane of the material as (−1 1 1) and (1 1 1) corresponding to the 2θ values of 35.55° and 38.82° which are attributed to monoclinic structure. These results agree with

the JCPDS data for CuO (Card No: 05-0661). No other peaks were observed revealing the absence of cuprous oxide or any other impurities. Fig. 2(b) shows the XRD patterns of the CuO thin films annealed at a temperature of 200 °C. The relatively broader diffraction peaks suggest the formation of smaller crystallites at the earlier stages. With the increase of the deposition cycles (20–60), slightly narrowed diffraction peaks appear, suggesting a small increase in the crystallite size. At this point the peak intensity increases whereas the peak width decreases. Silver nanoclusters were deposited over the as prepared and annealed CuO films using thermal evaporation technique. The XRD patterns of the Ag@CuO annealed films obtained with different deposition cycles are shown in Fig. 2(c). The positions of all the peaks are in agreement with the JCPDS data for CuO (Card No: 04-0783). The values of the average grain size of the as-prepared CuO films, calculated using Debye Scherrer formula, were in the range of 10 and 16 nm (Fig. S1). Similarly from Fig. S2, the average grain size is observed to increase upon annealing at 200 °C, which is a consequence of the merging process induced from thermal annealing. The grain boundaries of CuO nanoparticle vary due to the dangling bonds related to the copper containing oxygen defects. These defects help in the merging process to form larger CuO grains on annealing [21]. It is also found that the Full width half maximum (FWHM) value exhibits a tendency to decrease on annealing, which can be attributed to the merging of the grains on annealing. Hence, the crystallinity of the CuO thin films is found to improve on annealing. This may be due to the crystallites gaining enough energy to orient in proper equilibrium sites on annealing, resulting in improvement of crystallinity with the degree of orientation within the CuO films. These variations persist for CuO thin films deposited after 20, 40 and 60 reaction cycles. Thus the XRD analysis indicates the formation of high purity single phase CuO nanostructures with a monoclinic structure.

3.2. Morphology of pure CuO nanostructured thin film and their wettability

Copper hydroxide $Cu(OH)_2$ is a metastable phase which easily transforms into the more stable copper oxide, CuO. This transformation occurs in solid state by thermal dehydration at a relatively low temperature, and also in aqueous media at room temperature. The copper hydroxide resembles a sheet-like structure. The 2D layers of these sheets parallel to the (0 1 0) plane and are connected by H-bonds. When the substrates are immersed in hot water at 80 °C, the as-formed $Cu(OH)_2$ loses H_2O molecules due to the breaking of interplanar H-bonds, since it will not be stable at high

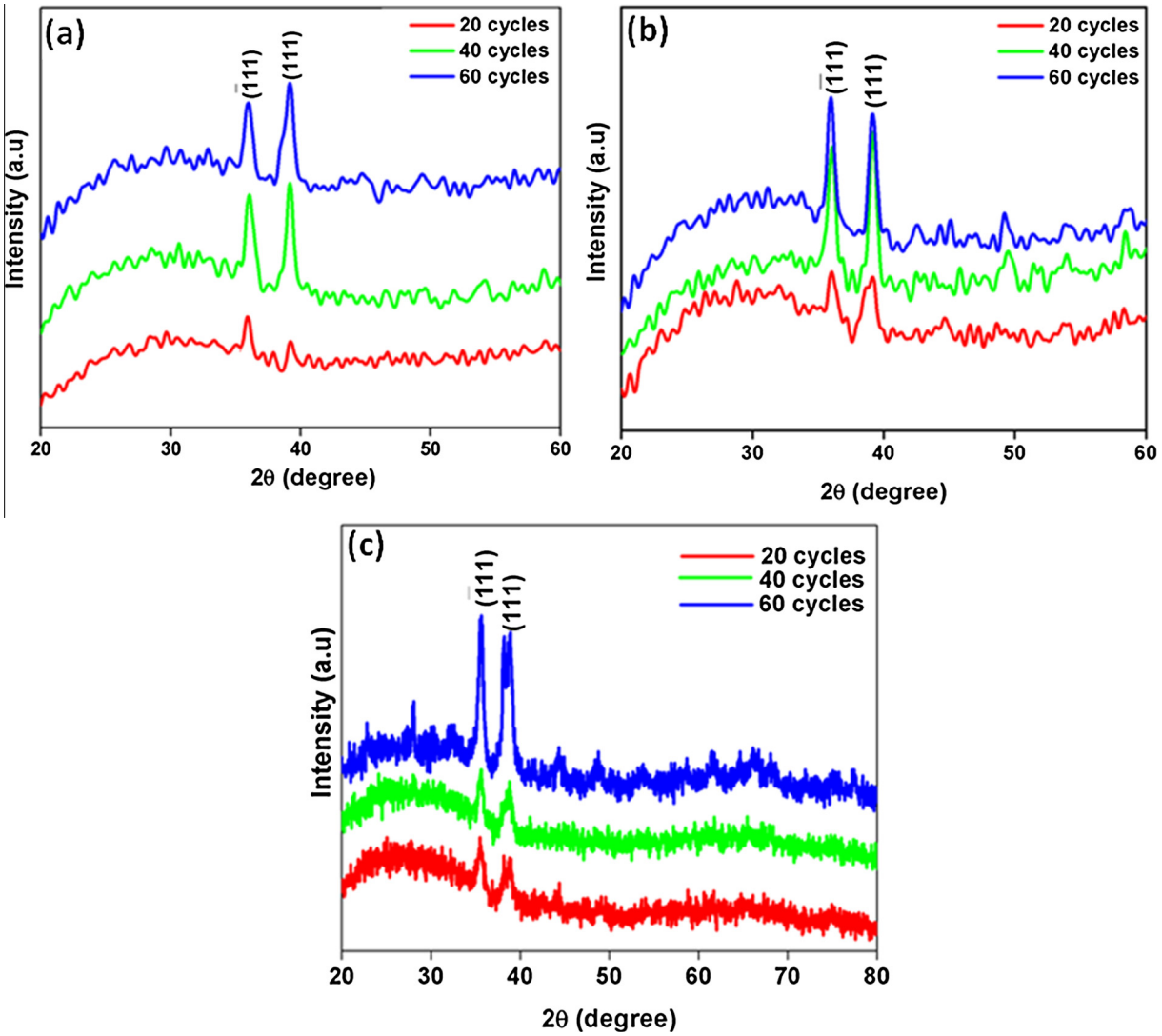

Fig. 2. XRD spectra of CuO thin films for 20, 40 and 60 cycles (a) As-prepared samples. (b) Annealed at 200 °C. (c) Ag@CuO thin films for 20, 40, and 60 annealed cycles.

temperatures consequently accelerating the dehydration rate. This results in rupturing of the bond in $Cu(OH)_2$ which breaks down into CuO and H_2O, forming CuO nanoparticles [22]. Hence the formation of nanospindles is attributed to the orderly arrangement of small nanoparticles (Fig. S3(a–e). Fig. S3(f–h) shows the formation of CuO nanospindles by successive deposition cycles, which indicates that the nanospindles become denser with increase in the number of deposition cycles.

Several factors, including electrical and dipolar fields, van der Waals forces, and hydrogen bonds may have various effects on the self-assembly [23]. Subsequently, the CuO nanoparticles, serving as the building blocks, self-assemble along identical directions. With this oriented attachment processes continuing via repeated deposition, some lateral attachments of CuO nanoparticles also appear along the width direction by slow growth. The growth rates via the oriented attachment along the length and width directions are very different and hence the spindle-like CuO architecture is finally obtained.

Accordingly, the possible growth mechanism for the formation of the flower-like CuO structure and silver decorated copper oxide nanoflowers is schematically illustrated in Fig. 3. Initially, when the reaction was performed with 20 cycles, a small number of spindles were formed as shown in Fig. 4(a), with a contact angle of 27.9°. When the reaction was extended to 40 cycles, the spindles became thicker and denser as presented in Fig. 4(b), while the water contact angle increased to 44.5°. The same process was carried out for 60 cycles so that an even distribution with increased number of spindles resulted which was super hydrophobic with an angle of 82.5° (Fig. 4(c)). These results give the obvious evidence for the formation of CuO nanospindles through the oriented attachment of small nanocrystals. Finally, the obtained CuO spindles self-assembled with each other to form CuO nanoflower structures with the long axes pointing towards a common centre forming a more thermodynamically stable configuration when annealed at 200 °C. Here it is clearly visible that after annealing, the edges of the petals become sharp, narrow and uniformly distributed over the substrates. The samples annealed at 200 °C for 60 cycles show the maximum superhydrophobicity (WCA ~ 157.9°) and resemble complete flower like structures as shown in (Fig. 4(f)) and inset Fig. 4(g).

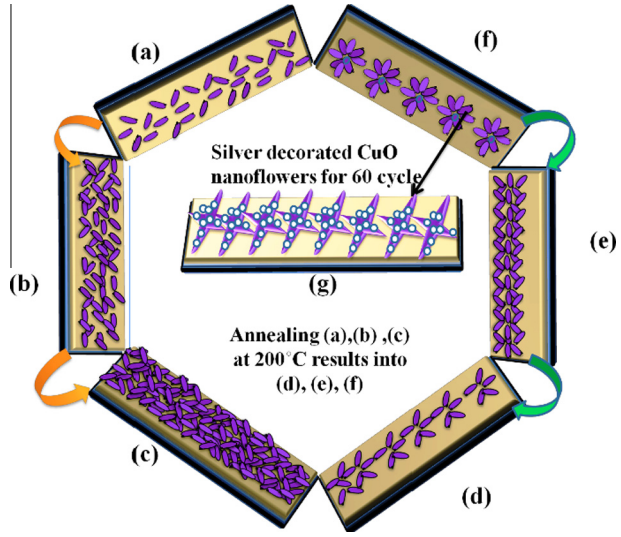

Fig. 3. Schematic illustration for the growth mechanism of CuO nanoflowers for different cycles: (a) Leaf like structure (20 cycles), (b) dense nanoleaves (40 cycles), (c) nanobuds 60 cycles annealing at 200 °C, (d) self assembled nanoleaf 20 cycles, (e) orderly arranged leafs (40 cycles), (f) nanoflower array (60 cycles), (g) silver deposited CuO nanoflowers.

3.3. Morphology analysis of Ag@CuO films and their wettability

The FESEM images of the Ag@CuO thin films are shown in Fig. 5 (a–f). The morphology of the Ag@CuO substrate shows aggregated and randomly arranged nanoclusters like structure. The contact angle for the CuO nanospindles shows small variation with a decrease in a contact angle from 27.9° to 24.3° for 20 cycles and similarly for 60 cycles it varies from 82.5° to 80.5° with respect to pure sample respectively. From the images (Fig. 5(a–c)) of the as-prepared samples, it is clearly visible that the areal coverage and particle size of Ag are very small and more circular clusters are obtained and on annealing, these clusters start to merge. The annealed samples (Fig. 5(d–f)) tend to be more elongated and have a broader distribution of particles as compared to the as-prepared samples. These results reveal that the Ag nanoparticles are uniformly coated on the surface of CuO nanoflowers as shown in inset Fig. 5(g), and the superhydrophobic nature still remains with an angle of 150°4 for 60 cycle deposition. Especially, the interparticle distance of these silver nanoparticles is small due to the densely arranged CuO nanoflowers and the aggregations of Ag nanoparticles are high on these flowers resulting in a cone like morphology. So, many hot spots occur and hence a large electromagnetic enhancement is expected on this substrate.

3.4. XPS analyses

The XPS analysis for the Ag@CuO thin film (Fig. 6(a)) shows a high symmetry corresponding to the position of Cu 2p1/2 and Cu 2p3/2 peaks centered at the binding energy values of 954.3 and 934.2 eV, respectively. The calculated difference in binding energy (23 eV) corresponds to the characteristic value for CuO and the absence of binding energy peaks of metallic Cu confirms the existence of Cu in oxidized states only [24]. The XPS curves of Ag 3d region in Fig. 6(c) have doublet Ag 3d5/2 and Ag 3d3/2 peaks with a low intensity ratio of 3:2 due to the deposition time of 2 min, located at 373.92 and 379.90 eV respectively. The EDX spectrum confirms that the prepared samples are composed of the elements Ag, Cu and O. The signals of both Cu and O are attributed to the CuO nanoflowers. The Ag signal arises from the Ag film on the surface of the CuO nanoflowers. The presence of Ag is negligible due to low deposition rate of silver nanoparticles. However, the atomic weight percentage of silver was confirmed by EDX analysis as 2.31% (Fig. S4). The intensity of silver is very weak and CuO suppresses the peak even after a deposition time of 5 min. The comparison of Ag 3d peak of Ag@CuO with the pure metallic silver sample shows the characteristic of metallic silver with the Ag 3d peak appearing at a binding energy of 373.92 eV and with a separation of 5.9 eV between Ag 3d5/2 and Ag 3d3/2 doublet peaks. The binding energy of Ag in the Ag@CuO composites is lower than that of zero valent Ag, indicating the transfer of electrons from Ag nanoparticles to CuO nanoflowers. Thus the XPS analysis further confirms the formation of nanocomposites between CuO and Ag.

3.5. UV–Visible analysis

When compared to the UV–vis spectra of CuO, the absorption peak between 300 and 400 nm of the Ag@CuO has blue shifted (Fig. 7). Since Ag was coated onto the CuO it may act as the molecular link between the nanostructures of CuO. Hence strong interfacial coupling occurs, leading to the blue shift of surface plasmon absorption (SPR) peak. This is attributed to the CuO thin film (formed with 60 growth cycles) which has well defined and densely packed nanoflowers. When silver nanoparticles come into contact with a p-type semiconductor (CuO), electrons flow from Ag to CuO for the equilibration state of the fermi level between the two. This phenomenon occurs because the work functions of

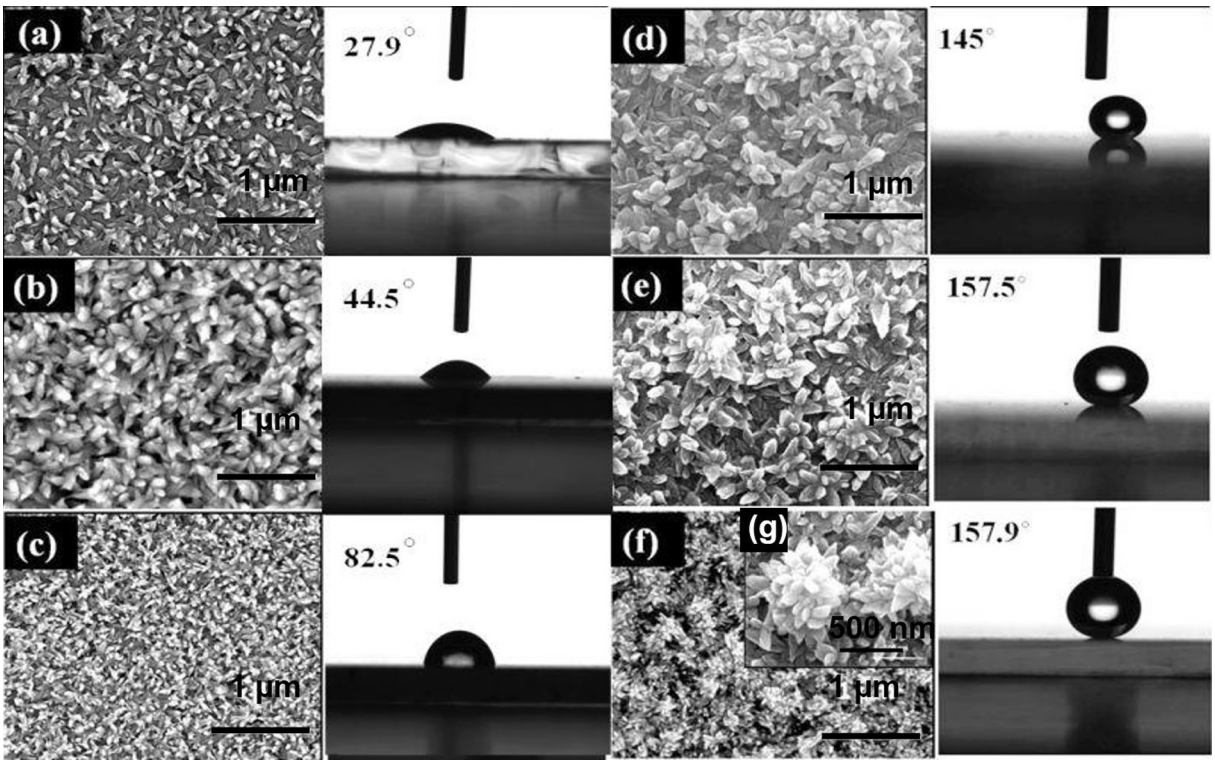

Fig. 4. Morphology and wettablity behaviour of CuO nanostrctured thin film prepared at different deposition cycles. (a) 20 (b) 40 (c) 60 cycles represents as deposited films and annealed films at 200 °C represent by (d) 20(e) 40 (f) 60 cycles respectively, (g) inset figure shows nano flower like structure.

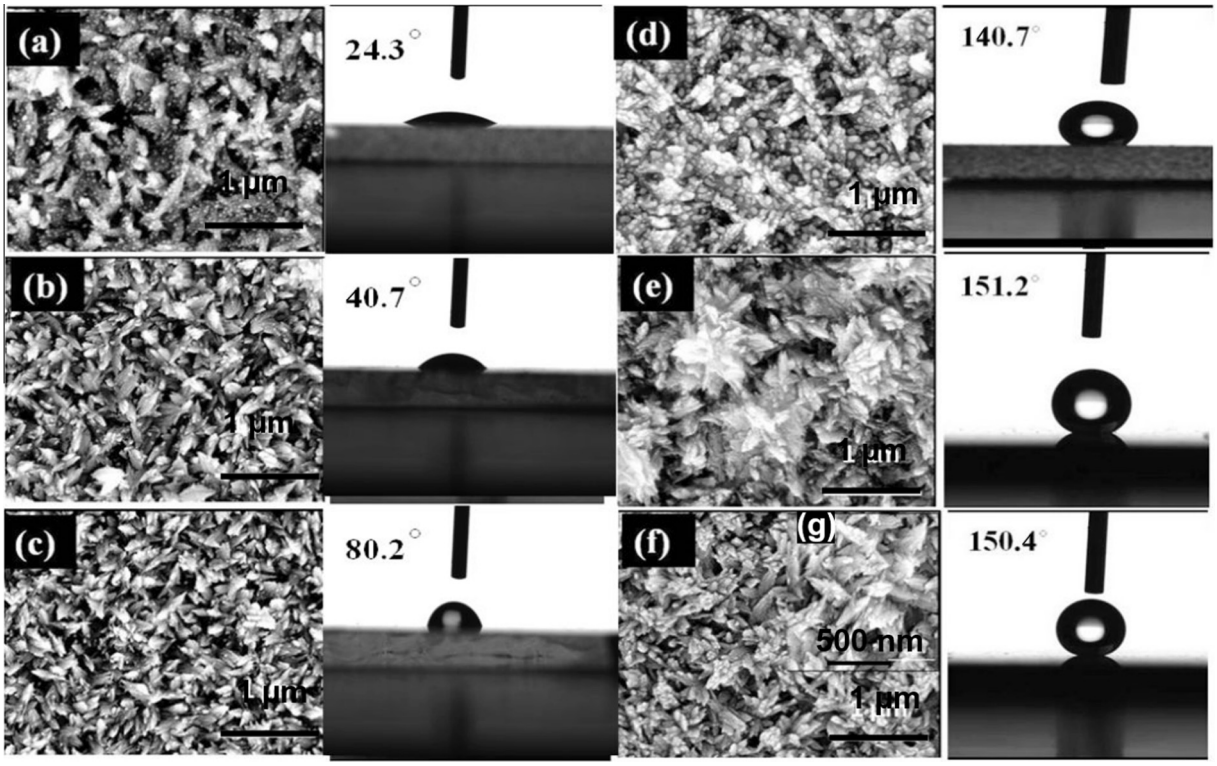

Fig. 5. Morphology and wettablity behaviour of Ag@CuO thin film for prepared ar different deposition cycles (a) 20 (b) 40 (c) 60 as deposited and annealed films at 200 °C (d) 20 (e) 40 (f) 60 cycles respectively, (g) inset figure shows nano flower like structure.

Ag (4.1 eV) [25] is lower than that of CuO (5.3 eV) [24]. It also deforms the bands (valence and conduction) of CuO to move relatively down to the fermi level. The junction of positively charged Ag particles and negatively charged CuO nanoparticles may induce a larger electromagnetic field, so that the Ag clusters film would excite a more intense LSPR on irradiation with a suitable laser, which is one of the important parameters for a substrate to be SERS active.

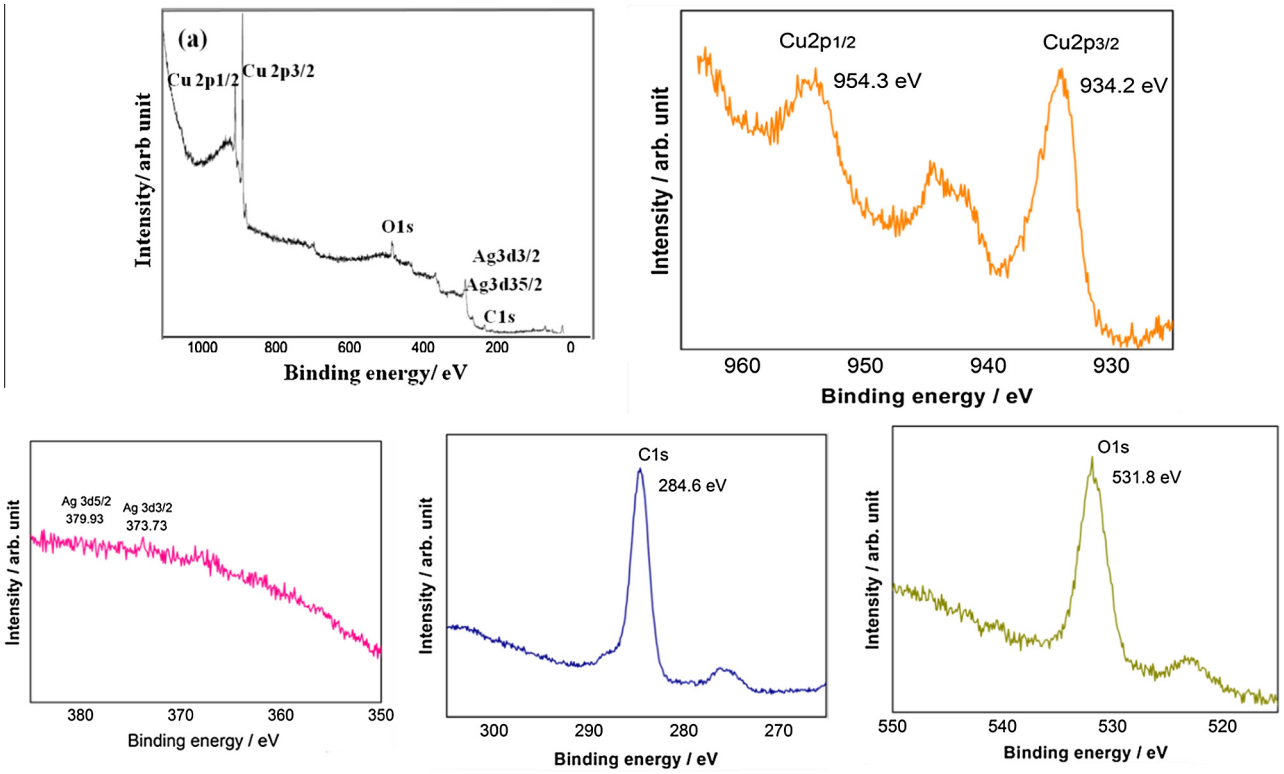

Fig. 6. XPS spectra (a) Ag@CuO nanoflowers (b–e) corresponding magnified spectra of individual elements (b) copper, (c) silver, (d) carbon, (e) oxygen.

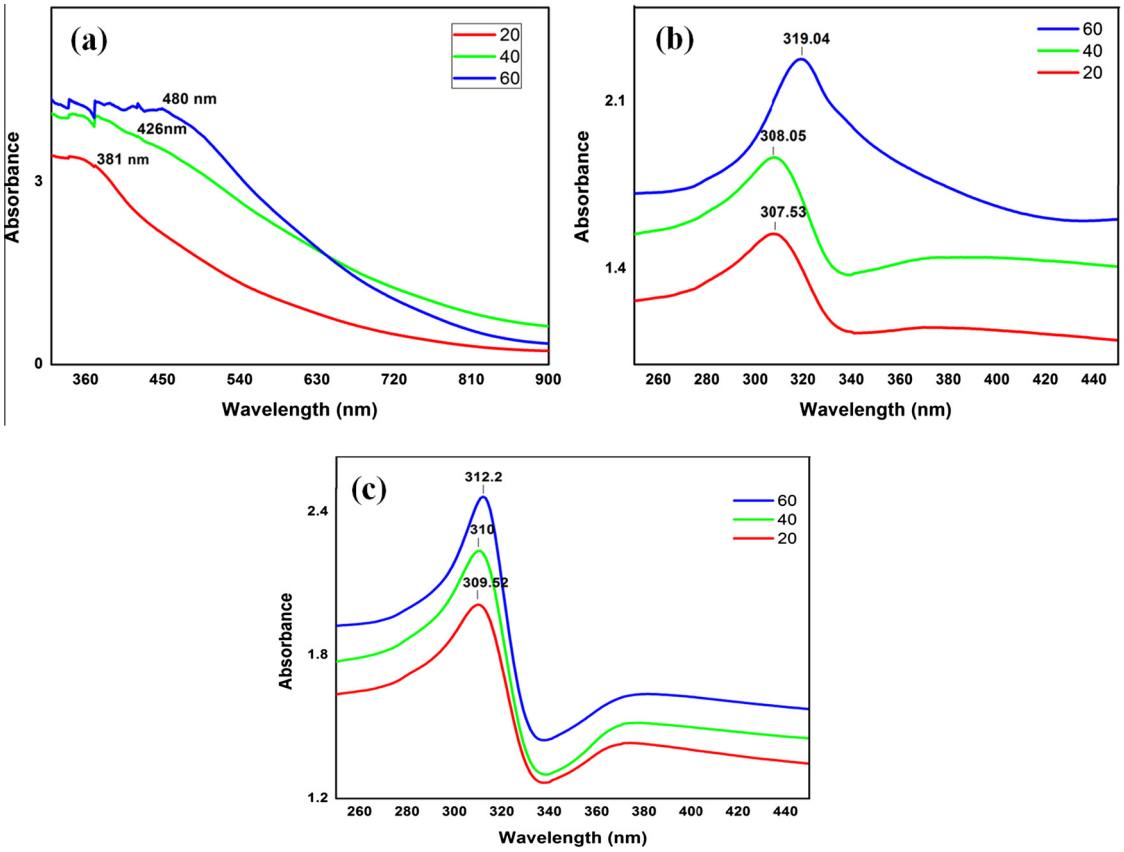

Fig. 7. UV–visible spectra of (a) pure CuO and (b) Ag@CuO nanostructure thin films (c) absorption spectrum of Ag film.

4. SERS of Ag@CuO nanostructures

The SERS activity was characterized using Rhodamine 6G as the target probe molecule with serial dilution from 10^{-9} to 10^{-12} M. Liquid solution of R6G shows Raman signals at 610.23, 772, 1184, 1362, 1507, 1571 and 1648 cm^{-1} with 514.5 nm laser source as shown in Fig. 8 for 10^{-9} M for all cycles. Initially SERS performance of the as-prepared Ag@CuO thin films after 20 reaction cycles was investigated with different concentrations (10^{-9} to 10^{-12} M) of R6G solution on them (Fig. 8(a–c)). The characteristic peaks (Fig. 9) of R6G molecules and their intensities have been discussed in Table S2, which strongly depend on super hydrophobicity and Ag deposition. These peaks are assigned to the xanthene ring stretch, ethylamine group and carbon–oxygen stretch of R6G [26].

The 614 cm^{-1} peak corresponds to the C—C—C ring in-plane bending mode. The C—H out-of-plane bending mode for R6G is observed at 771 cm^{-1} while the C—O—C stretching frequency appears at 1187 cm^{-1}. Peaks centered at 1362, 1507, 1571 and 1648 cm^{-1} are attributed to the aromatic C—C stretch of the R6G molecule. The spectrum band intensities show a significant downward trend with the decline in the concentration of the analyzed probe molecule. Further experiments for 40 and 60 reaction cycles were also done (Fig. 9(b and c)). It should be noted that the Raman signals are relatively weaker for very low concentration (10^{-11}–10^{-12}). The intensity of Raman peaks of R6G molecules on the substrate decreases as concentration is decreased, accompanied by a position shift and peak shape change, and the characteristic peak eventually vanishes. The decrease in the peak intensity is related to the reduced number of the R6G molecules in the collection volume of the Raman spectroscope. The change in peak shape and the shift in peak position are related to the change in the chemical bonding of the R6G molecules due to interactions between the molecules and the environment [27,28]. The spectral intensity of R6G on annealed Ag@CuO thin films shows improved SERS performance as compared to the as prepared counterparts from Fig. S5. The SERS activity of the as-prepared substrate improves with annealing at 200 °C and an increase in Raman intensity is obtained for all the reaction cycles. Owing to the nanostructure of Ag nanoclusters decorating the surfaces of CuO nanoflowers, the integration of the electromagnetic enhancement effect arises from the surface plasma resonance of the Ag NPs due to the chemical enhancement properties of the

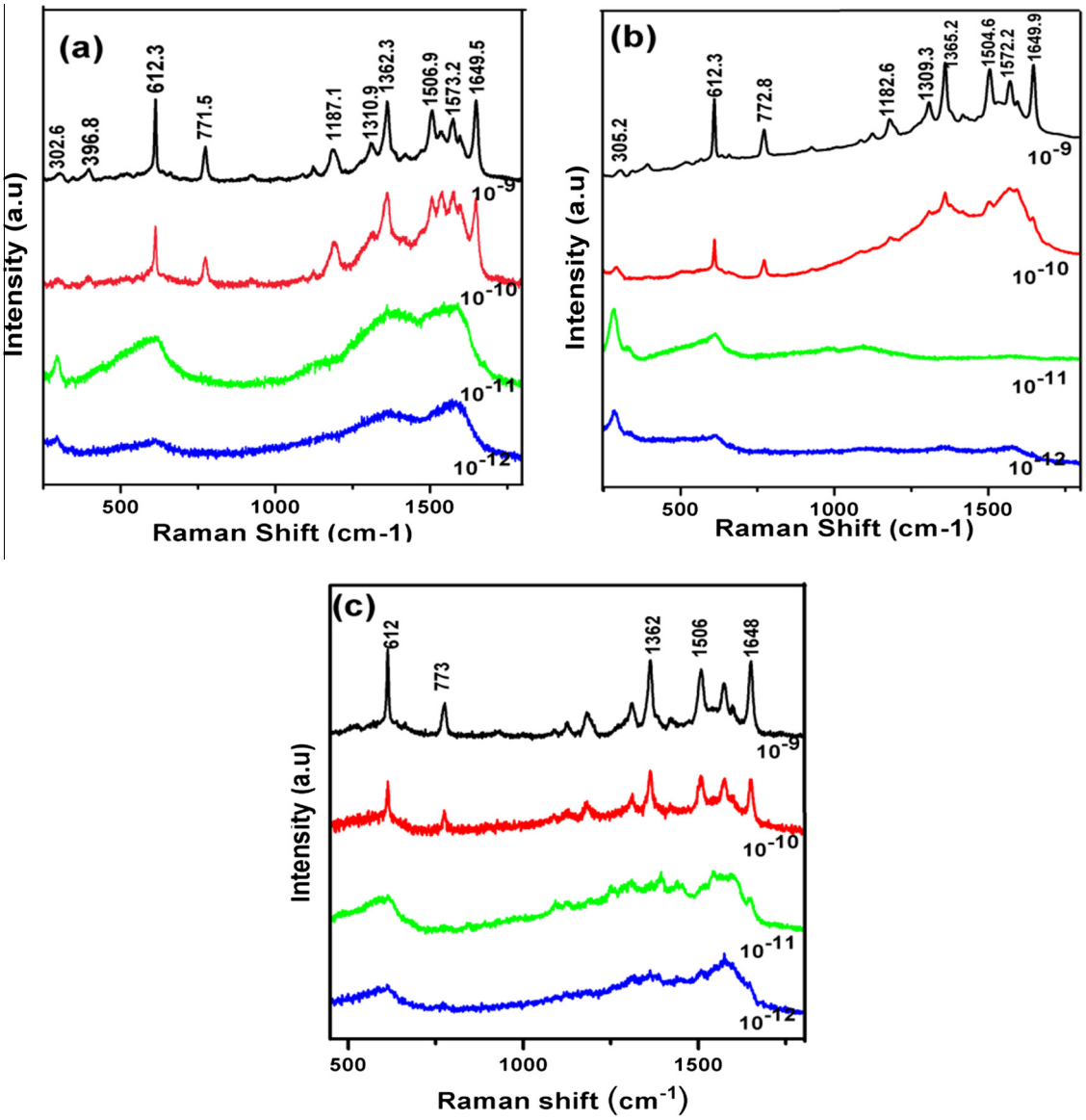

Fig. 8. SERS spectra for the as-prepared Ag@CuO thin films for (a) 20, (b) 40, and (c) 60 reaction cycles.

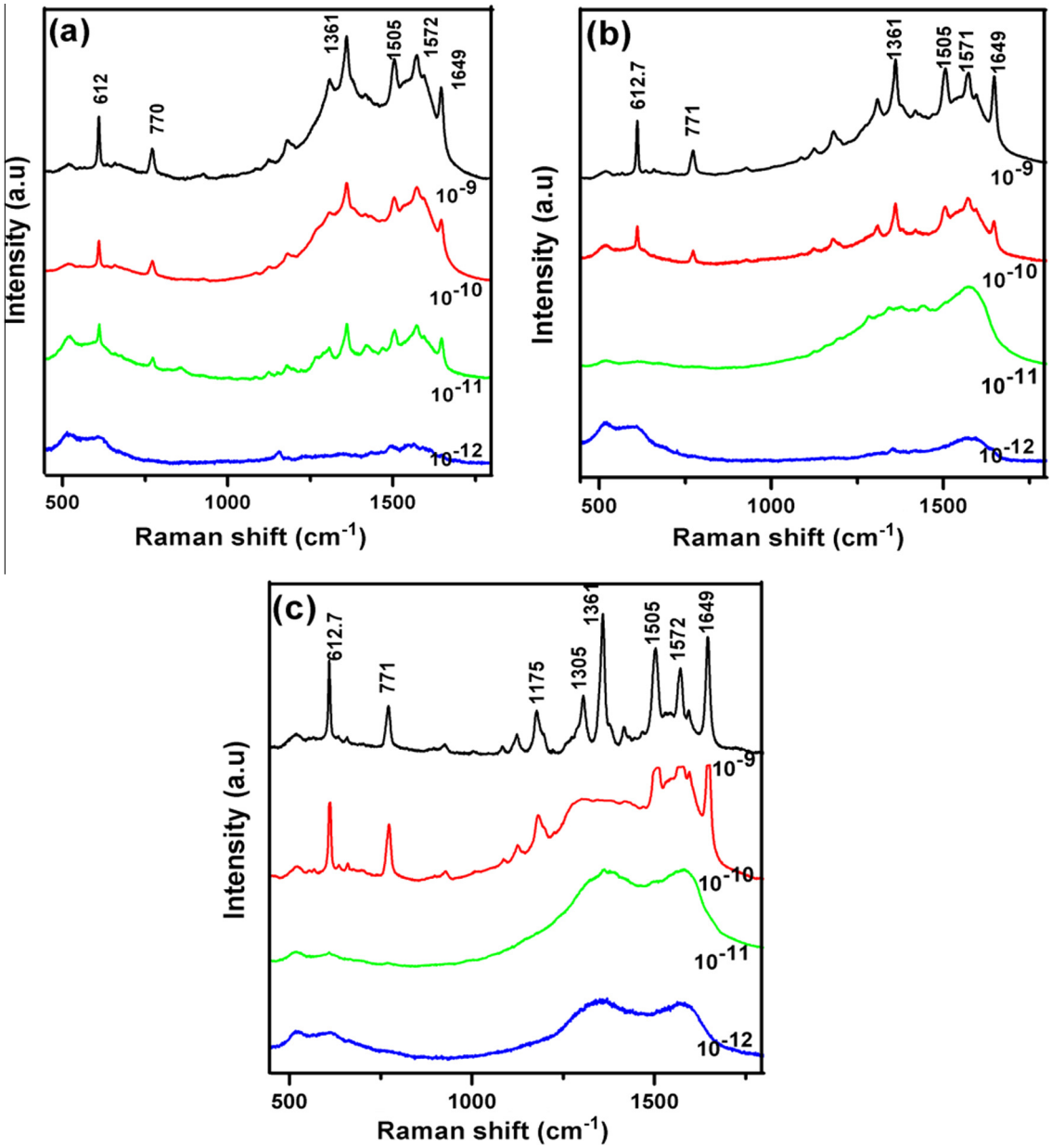

Fig. 9. SERS spectra of annealed Ag@CuO thin films for (a) 20, (b) 40 and (c) 60 reaction cycles.

CuO nanoflowers which could extend the detection limit of the substrates up to 10^{-10} M. Comparing with the Raman spectra, it is obvious that the Ag@CuO nanoflowers exhibit the highest SERS enhancement ability.

4.1. Estimation of SERS enhancement factor

For SERS performance, Ag was deposited on CuO thin films with a thickness of 100 nm. The SERS activity of the Ag-NP-decorated samples was evaluated using 20 μl volume of R6G dye molecule with molarity varying from 10^{-12} M to 10^{-9} M. The characteristic peaks of R6G molecules and their intensities strongly depend on superhydrophobicity with water contact angle of 150.4 after Ag deposition as shown in Table S1. The enhancement factor (EF) for SERS is determined to be of the order of 10^7 for the R6G peaks at 610 by using the formula [29].

$$EF = \frac{I_{SERS}}{I_{bulk}} \times \frac{N_{bulk}}{N_{surf}}$$

The above calculation is well illustrated in Fig. S7. In the present work, for the confirmation of field distribution, the finite-difference time-domain (FDTD) method is adopted using lumerical solution-8. Intensity ($\langle|E|^2\rangle$) distributions are obtained from 2D FDTD calculations based on the following parameters: CuO palik material has been used, where the SEM whole image is used for 2D simulation work for Laser with 514 nm wavelength. The detailed process is illustrated in Fig. S6. The maximum intensity ($\langle|E|^2\rangle$) of each noble metal/semiconductor was 167.96 V/m. As the SERS signals were proportional to the value of ($\langle|E|^2\rangle$), the Ag@CuO nanoflowers substrates for 60 cycles showed SERS enhancement comparable to pure CuO nanoflowers films due to the very low thickness of the silver film. The comparative SERS enhancement has been calculated in Table 1 as the Raman intensities for Figs. 8 and 9 give the impression of being similar. A comparison with other methods with respect to the detection limit and the water contact angles is given in Table 2 respectively. The present morphology has high impact on SERS studies using superhydrophobic films.

Table 1
SERS enhancement Factor for Ag@CuO nanostructured thin film.

Peak position – 612.7 cm^{-1}				
Growth cycles	Intensity for 10^{-10} M (I_{SERS})	Intensity for 10^{-3} M (I_{Bulk})	I_{SERS}/I_{Bulk}	Enhancement factor
20 – as prepared	908.09	47.300	19.19	6.26×10^6
20 – annealed	1631.9	47.300	34.50	1.12×10^7
40 – as prepared	382	47.300	8.07	2.63×10^6
40 – annealed	2830	47.300	59.83	1.93×10^7
60 – as prepared	451.47	47.300	9.544	2.12×10^6
60 – annealed	2908.54	47.300	61.491	2.0×10^7

Table 2
Comparative Table for different metal oxides for SERS studies on the basis of methodology and enhancement factor.

S. no	Obtained nanostructures	Dye used and detection limit	Method used & water contact angle	Enhancement factor	Ref
(1)	Zinc oxide nanorods array	4-ATP 5 μl	Chemical bath deposition 152°	–	[2]
(2)	Ag@ZnO worm like Morphology	R6G 10^{-10} M	Vacuum coating 155°	3.082×10^7 M	[3]
(3)	Ag-Cu SERS substrate	R6G 5×10^{-6} M	Galvanic displacement reaction Not defined	330 times	[5]
(4)	copper microcages	R6G 10^{-6} M	Chemical reduction Not defined	–	[12]
(5)	Cu nanoparticle-coated copper vanadate nanoribbons	R6G 10^{-9} M	Hydrothermal method Not defined	1.6×10^6	[18]
(6)	Ag@CuO nanoflower film	R6G 10^{-10} M	SILAR Method 150°4	2×10^7	Present method

4.2. Role of wettability on SERS

In order to study the surface wettability behaviour of the Ag@CuO nanostructured thin films grown with different growth cycles the water contact angle (CA) was measured as shown from Fig. 8. When silver nanoparticles were deposited on the CuO thin film, water CA values from 140° to 151° for the samples prepared with different growth cycles as shown in Table S1. The water contact angle on this substrate decreases slightly from the contact angle of pure CuO thin films. Fig. 10(a) shows the variation of CA with the number of reaction cycles and Fig. 10(b) shows photographic images of water drops on the surface of the silver coated CuO nanoflowers. The superhydrophobicity of annealed samples are greater than that of the as deposited samples (Table S1 and Fig. 4). The 60 cycle film was annealed till it attains its superhydrophobicity with an angle of 156.4 on silver deposition (Fig. 5 (f)). One of the distinctive properties of the hydrophobic surface is that it has the ability to reduce the contact area between the droplet and the underlying surface below the hydrophilic surface. Thus the diluted probe molecules in the droplet will be highly concentrated after the droplet dried on the super hydrophobic surface. This is known as the hydrophobic condensation effect [2], which may further amplify the SERS signal to achieve more sensitive detection.

4.3. Mechanism of SERS enhancement by Ag@CuO nanoflowers

The higher SERS enhancement for Ag@CuO nanoworms may be due to the following reasons. The Inter and intra CuO nanoflower arrangement produce an electric field (Fig. 11(a)) due to the silver deposition where the Inter silver nanoparticles give larger enhancement [30]. Also, a depletion layer may be formed at the interface between CuO and Ag due to the different work functions [24], which reduces the rate of recombination. Thus, charge

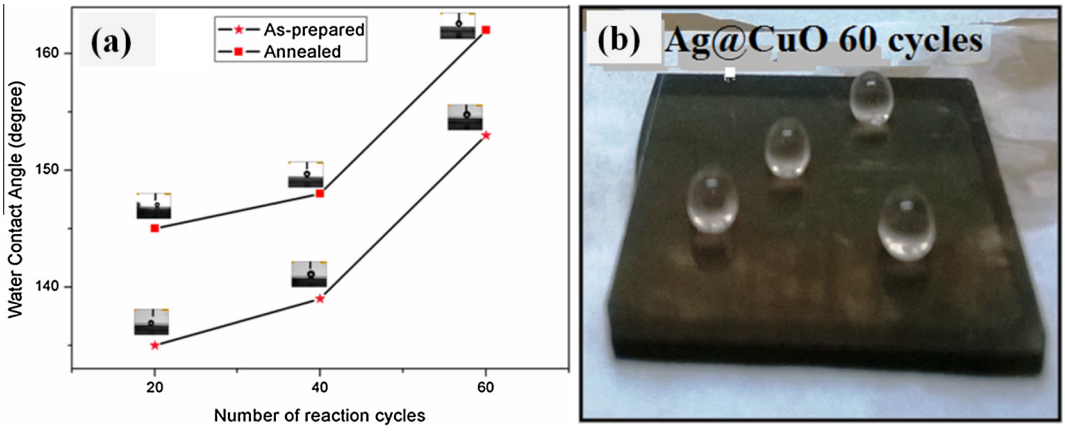

Fig. 10. (a) A plot of water contact angle against number of reaction cycles indicating the hydrophobic behaviour of CuO thin films. (b) Real images of annealed silver decorated CuO nanoflower thin for 60 cycle.

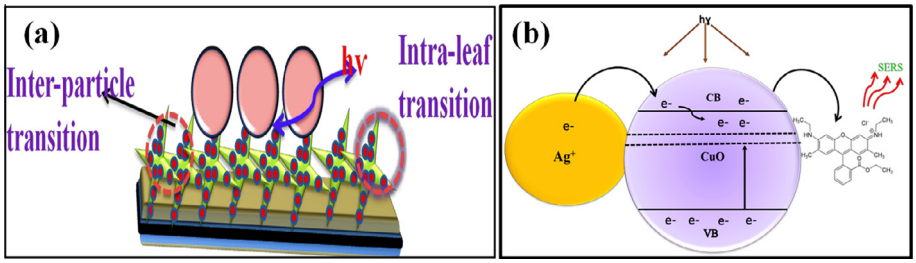

Fig. 11. Charge transfer mechanism between Ag@CuO nanostrctured films for R6G dye molecules. (a) The inter and intra CuO nanoflower arrangement. (b) HOMO and LUMO energy levels of R6G under excitation.

transfer occurs from Ag to CuO with 514 nm excitation. The changed electromagnetic intensity of the Ag@CuO nanoflowers is the main reason for SERS enhancement.

The best results are obtained for super hydrophobic (157°) 60 cycle films that correspond to randomly arranged Ag@CuO nanoflowers. The SERS spectra of each sample vary with the variation of water contact angle from 140.7 to 150.4°. SERS is significantly promoted when the substrate shows the superhydrophobicity at 156.4° as a result of surface energy and capillary force. In the case of randomly arranged nanostructures, the most significant SERS enhancement occurs due to inter and intra CuO nanoflower arrangement and inter silver nanoparticles deposition.

As shown in Fig. 11(b), introducing an R6G molecule onto the Ag@CuO thin film makes it possible to build a complete charge transfer (CT) system of "donor-bridge-acceptor" due to the Fermi level of silver being lower than the surface state energy level of CuO [31]. When an Ag particle is in contact with a p-type semiconductor particle such as CuO, the charge distribution is readjusted for equilibration of the Fermi level between the two particles, which results in the elevation of the Ag Fermi level and the formation of a Schottky barrier (depletion layer) at the junction between the two materials. Silver nanoparticles on the CuO thin film surface were excited by incident laser light and the photoexcited electrons which were injected into the conduction band of CuO connect with Ag and migrate towards lower energy levels of the conduction band of CuO. These electrons are then transferred to the LUMO orbits of the molecules adsorbed on CuO nanoparticles, which enhances photo absorption of the charge transfer complex. These additional electrons provide CuO with a considerable SERS effect to the adsorbed molecules. Besides this dynamic charge transfer, intrinsic charge transfer also occurs from CuO-to-R6G and R6G-to-Ag when the energy levels of the system match the highest occupied molecular orbital (HOMO) and lowest unoccupied molecular orbital (LUMO) energy levels of R6G under excitation. This indicates that an appropriate amount of surface deposited Ag can play a vital role to improve the SERS effect of CuO to surface adsorbed molecules which is induced by the CuO-to-R6G molecule charge transfer.

5. Conclusions

The present technique is a facile SILAR approach towards fabrication of low cost active SERS substrates consisting of super hydrophobic nanoflowers arrays. The substrates exhibit an ideal reproducible surface morphology where strong SERS signals can be generated from minimal quantities of adsorbed analyte. The optical properties were studied for CuO and Ag@CuO nanoparticles. The peak position shows that Ag coated CuO has strong Plasmon resonance. The growth mechanism of nanoflowers array was represented via morphological imagery, where the nanospindles were formed in the initial deposition cycles. Furthermore, the detection of R6G was demonstrated for lower concentrations (10^{-10} M), and the Raman intensities exhibited a linear relationship towards concentration and played a potential role for trace analysis of R6G dye. The enhancement factor was found to be of the order of 2×10^7. The present study may provide a new perception in the fabrication of super hydrophobic substrates for SERS, which could be further used for pesticides detection in foods and can also act as a glucose detector in biosensor applications. The above results also provide a new opportunity for SERS substrate to explore molecule–semiconductor interaction.

Appendix A. Supplementary material

Supplementary data associated with this article can be found, in the online version, at http://dx.doi.org/10.1016/j.jcis.2016.05.051.

References

[1] Q.X. Zhang, Y.X. Chen, Z. Guo, H.L. Liu, D.P. Wang, X.J. Huang, ACS Appl. Mater. Inter. 5 (2013) 10633–10642.
[2] F. Xu, Y. Zhang, Y. Sun, Yan Shi, Z. Wen, Z. Li, J. Phys. Chem. C 115 (2011) 9977–9983.
[3] N.D. Jayram, S. Sonia, S. Poongodi, P. Suresh Kumar, Yoshitake Masuda, D. Mangalaraj, N. Ponpandian, C. Viswanathan, App. Surf. Sci. 355 (2015).
[4] S. Bhavya, R.F. Renee, I.H. Anne, R. Emilie, R.P. Van Duyne, Mater. Today 15 (2012) 16–25.
[5] L. Chen, Z. Zhang, G. Chen, C. Lai, Hui Zhou, AIP Adv. 4 (2014) 031324–031328.
[6] N. Zhou, V. Lopez-Puente, Q. Wang, L. Polavarapu, I. Pastoriza-Santos, Q.H. Xu, RSC Adv. 5 (2015) 29076–29097.
[7] V.E. Subramanian, E. Wolf, P.V. Kamat, J. Phys. Chem. B 105 (2001) 11439–11446.
[8] X.Q. Wang, T.J. He, H. Wen, C.Y. Xu, J. Zuo, F.C. Liu, Spectrochim. Acta, Part A 53 (1997) 2495–2504.
[9] A.A. Kowalska, A. Kaminska, W. Adamkiewicz, E. Witkowska, M. Tkacz, J. Raman Spectrosc. 46 (2015) 428–433.
[10] M. Achermann, J. Phys. Chem. Lett. 1 (2010) 2837–2843.
[11] L. Yang, J. Lv, Y. Sui, W. Fu, X. Zhou, J. Ma, S. Su, W. Zhang, P. Lv, D. Wu, Y. Mu, Haibin Yang, Cryst. Eng. Comm. 16 (2014) 2298–2304.
[12] C. Kong, S. Sun, X. Zhang, X. Song, Z. Yang, Cryst. Eng. Comm. 15 (2015) 6136–6139.
[13] H.G. Yu, J.G. Yu, S.W. Liu, S. Mann, Chem. Mater. 19 (2007) 4327–4334.
[14] L.J. Xie, W. Chu, J.H. Sun, P. Wu, D.G. Tong, J. Mater. Sci. 46 (2011) 2179–2184.
[15] Y. Wang, H. Hu, S. Jing, Y. Wang, Z. Sun, B. Zhao, C. Zhao, J.R. Lombard, Anal. Sci. 787 (2007) 23787–23793.
[16] Z. Mao, W. Song, L. Chen, W. Ji, X. Xue, W. Ruan, Z. Li, H. Mao, S. Ma, R. Lombardi, B. Zhao, J. Phys. Chem. C 115 (2011) 18378–18383.
[17] S. Hsieh, P.Y. Lin, L.Y. Chu, Am. Chem. Soc 118 (2014) 12500–12505.
[18] H. Lin, Q. Shao, F. Hu, H. Wang, M. Shao, H. Lin, Q. Shao, F. Hu, H. Wang, M. Shao, Thin Solid Films 558 (2014) 385–390.
[19] P.S. Kumar, J. Sundaramurthy, D. Mangalaraj, D. Nataraj, D. Rajarathnam, M.P. Srinivasan, J. Colloid Inter. 363 (2011) 51–58.
[20] S. Sonia, Palaniswamy Suresh Kumar, Naidu Dhanpal Jayram, Yoshitake Masuda, D. Mangalaraj, Chongmu Lee, RSC Adv. 6 (2016) 24290–24298.
[21] L.B. Xia, W.Y. Yuan, W.Y. Fen, Acta Phys. Chim. Sinca 25 (2009) 2366–2372.
[22] D. Jundale, S. Pawar, M. Chougule, P. Godse, S. Patil, B. Raut, S. Sen, V. Patil, J. Sens. Tech 2 (2011) 5573–5584.
[23] S. Guiye, X. Lihong, W. Guorui, L. Yichun, J. Phys. Chem. C 111 (2007) 3290–3293.
[24] Y. Wang, W. Song, W. Ruan, J. Yang, B. Zhao, R. Lombardi, J. Phys. Chem. C 113 (2009) 8065–8069.
[25] W. Wang, Z. Feng, W. Jiang, J. Zhan, Cryst. Eng. Comm. 15 (2013) 1339–1344.

[26] S.K. Saikin, R. Olivares-Amaya, D. Rappoport, M. Stopa, A.J. Aspuru-Guzik, Phys. Chem. 11 (2009) 9401–9411.
[27] L. Yu, R. Pang, S. Tao, H. Yang, D. Wu, Z. Tian, J. Phys. Chem. A 117 (2013) 4286–4296.
[28] J. Chen, G. Qin, W. Shen, Y. Li, D. Biswajit, J. Mater. Chem. C 3 (2015) 1309–1318.
[29] N.D. Jayram, S. Sonia, P. Suresh Kumar, L. Marimuthu, Y. Masuda, D. Mangalaraj, N. Ponpandian, C. Viswanathan, S. Ramakrishna, RSC Adv. 5 (2015) 46229–46239.
[30] L. Jin, G. She, X. Wang, L. Mu, W. Shi, Appl. Surf. Sci. 320 (2014) 591–595.
[31] L. Yang, X. Jiang, W. Ruan, J. Yang, B. Zhao, W. Xu, R. Lombardi, J. Phys. Chem. C 113 (2009) 16226–16331.